

Optimizing COVID-19 control with asymptomatic surveillance testing in a university environment

Cara E. Brook^{1*}, Graham R. Northrup², Alexander J. Ehrenberg^{1,3,4,5}, the IGI Testing Consortium³, Jennifer A. Doudna^{3,6,7,8,9}, and Mike Boots^{1,10}

¹ Department of Integrative Biology, University of California, Berkeley

² Center for Computational Biology, College of Engineering, University of California, Berkeley

³ Innovative Genomics Institute, University of California, Berkeley

⁴ Helen Wills Neuroscience Institute, University of California, Berkeley

⁵ Memory and Aging Center, Weill Institute for Neurosciences, University of California, San Francisco

⁶ Department of Molecular and Cell Biology, University of California, Berkeley

⁷ College of Chemistry, University of California, Berkeley

⁸ J. David Gladstone Institutes, San Francisco, CA

⁹ Howard Hughes Medical Institute, University of California, Berkeley

¹⁰ Department of Biosciences, University of Exeter, Penryn, UK

*corresponding author: *Cara E. Brook*

address: 5017 Valley Life Sciences Building, University of California, Berkeley

phone: 707-241-5550

email: cbrook@berkeley.edu

1 **Abstract**

2 The high proportion of transmission events derived from asymptomatic or presymptomatic
3 infections make SARS-CoV-2, the causative agent in COVID-19, difficult to control through the
4 traditional non-pharmaceutical interventions (NPIs) of symptom-based isolation and contact
5 tracing. As a consequence, many US universities have developed asymptomatic surveillance
6 testing labs, to augment existing NPIs and control outbreaks on campus. We built a stochastic
7 branching process model of COVID-19 dynamics to advise optimal control strategies in a
8 university environment. Our model combines behavioral interventions in the form of group size
9 limits to deter superspreading, symptom-based isolation, and contact tracing, with asymptomatic
10 surveillance testing. We find that behavioral interventions offer a cost-effective means of
11 epidemic control: group size limits of six or fewer greatly reduce superspreading, and rapid
12 isolation of symptomatic infections can halt rising epidemics, depending on the frequency of
13 asymptomatic transmission in the population. Surveillance testing can overcome uncertainty
14 surrounding asymptomatic infections, with the most effective approaches prioritizing frequent
15 testing with rapid turnaround time to isolation over test sensitivity. Importantly, contact tracing
16 amplifies population-level impacts of all infection isolations, making even delayed interventions
17 effective. Combination of behavior-based NPIs and asymptomatic surveillance also reduces
18 variation in daily case counts to produce more predictable epidemics. Furthermore, targeted,
19 intensive testing of a minority of high transmission risk individuals can effectively control the
20 COVID-19 epidemic for the surrounding population. We offer this blueprint and easy-to-
21 implement modeling tool to other academic or professional communities navigating optimal
22 return-to-work strategies for the 2021 year.

23
24
25
26
27
28
29
30
31
32
33
34
35
36
37
38
39
40

41 Introduction

42 Non-pharmaceutical interventions (NPIs) to control the spread of infectious diseases vary
43 in efficacy depending on the natural history of pathogen that is targeted (1). Highly transmissible
44 pathogens and pathogens for which the majority of onward transmission events take place prior
45 to the onset of symptoms are notoriously difficult to control with standard public health
46 approaches, such as isolation of symptomatic individuals and contact tracing (1). SARS-CoV-2,
47 the causative agent in COVID-19, is a now a clear example of one of these difficult-to-control
48 pathogens (2). While the first SARS-CoV was effectively contained via the isolation of
49 symptomatic individuals following emergence in 2002 (3), at the time of writing, SARS-CoV-2
50 remains an ongoing public health menace that has infected more than 82 million people
51 worldwide (4). Though the two coronaviruses are epidemiologically comparable in their basic
52 reproduction numbers (R_0) (3), SARS-CoV-2 has evaded control efforts largely because the
53 majority of virus transmission events occur prior to the onset of clinical symptoms in infected
54 persons (2)—in stark contrast to infections with the first SARS-CoV (3). Indeed, in many cases,
55 SARS-CoV-2-infected individuals never experience symptoms at all (5–8) but, nonetheless,
56 remain capable of transmitting the infection to others (9–13). Due to the challenges associated
57 with asymptomatic and presymptomatic transmission (10), surveillance testing of asymptomatic
58 individuals has the potential to play a critical role in COVID-19 epidemic control (14–16).
59 Surveillance testing is always valuable for research purposes, but its efficacy as a public health
60 intervention will depend on both the epidemiology of the focal infection and the characteristics
61 of the testing regime. Here, we explore the effects of both behavior-based NPIs and
62 asymptomatic surveillance testing on COVID-19 control in a university environment.

63 As the North American winter advances, the United States leads the globe with over 21
64 million reported cases of COVID-19 (4), and universities across the nation continue to struggle
65 to control epidemics in their campus communities (17). To combat this challenge, colleges have
66 adopted a variety of largely independent COVID-19 control tactics, ranging from entirely virtual
67 formats to a mix of in-person and remote learning, paired with strict behavioral regulations,
68 and—in some cases—in-house asymptomatic surveillance testing (18). As we approach the 2021
69 academic semester, asymptomatic surveillance testing is likely to play a key role in university
70 plans for expanding reopening in the new semester (18, 19). In March 2020, shortly after the
71 World Health Organization declared COVID-19 to be a global pandemic (20), the University of
72 California, Berkeley, launched its own pop-up SARS-CoV-2 testing lab in the Innovative
73 Genomics Institute (IGI) (21) with the aim of providing COVID diagnostic services to the UC
74 Berkeley community and underserved populations in the surrounding East Bay region. Though
75 the IGI RT-qPCR-based pipeline was initially developed to service clinical, symptomatic
76 nasopharyngeal and oropharyngeal swab samples (21), the IGI subsequently inaugurated an
77 asymptomatic surveillance testing program for the UC Berkeley community, through which—at
78 the time of this writing—over 18,000 faculty, students, and staff in the UC Berkeley community
79 have since been serviced with over 105,000 tests and counting (22).

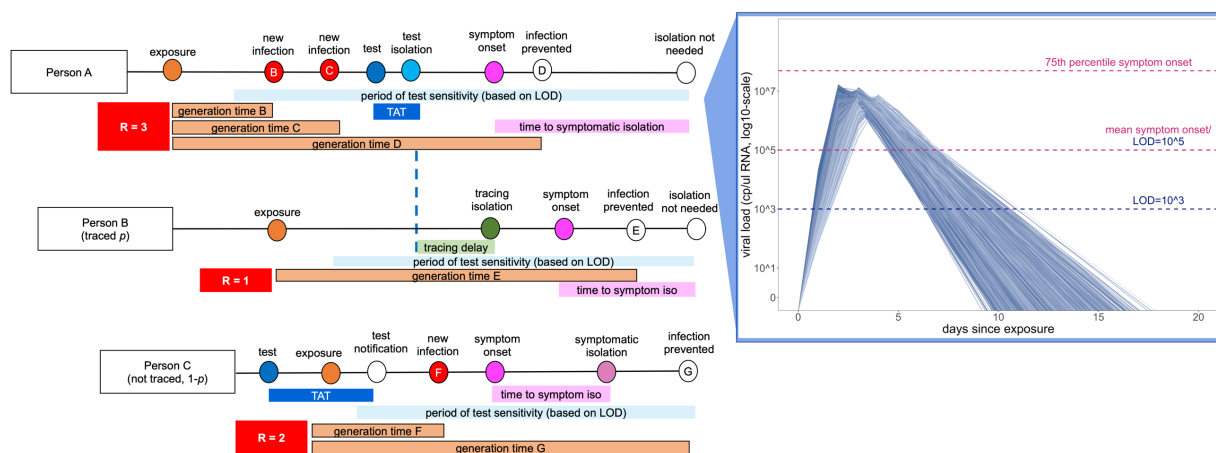
80 Here we developed a stochastic, agent-based branching process model of COVID-19
81 spread in a university environment to advise UC Berkeley on best-practice approaches for
82 surveillance testing in our community and to offer guidelines for optimal control in university
83 settings more broadly. Previous modeling efforts have used similar approaches to advocate for
84 more frequent testing with more rapid turnaround times at the expense of heightened test
85 sensitivity (14, 15) or to weigh the cost-effectiveness of various testing regimes against
86 symptom-based screening in closed university or professional environments (16). Our model is
87 unique in combining both behavioral interventions with optimal testing design in a real-world
88 setting, offering important insights into efficient mechanisms of epidemic control and an
89 effective tool to optimize control strategies.

90

91 **Model design.**

92 Our model takes the form of a stochastic branching process model, in which a subset
93 population of exposed individuals (0.5%, derived from the mean percentage of positive tests in
94 our UC Berkeley community (22)) is introduced into a hypothetical 20,000 person community
95 that approximates the campus utilization goals for our university in spring 2021. With each
96 timestep, the disease parameters for each infected case are drawn stochastically from
97 distributions representing the natural history of the SARS-CoV-2 virus, paired with realistic
98 estimates of the timeline of corresponding public health interventions (2, 16, 23) (Figure 1). Our
99 flexible model (published here with open-access R-code (24)) allows for the introduction of NPIs
100 for COVID-19 control in four different forms: (1) group size limits, (2) symptom-based
101 isolations, (3) surveillance testing isolations, and (4) contact tracing isolations that follow after
102 cases are identified through screening from symptomatic or surveillance testing. Because we
103 focus our efforts on optimal surveillance testing regimes, we do not explicitly model other NPIs,
104 such as social distancing and mask wearing; however, the effects of these behaviors are captured
105 in our representation of R-effective (hereafter, R_E) for both within-campus and out-of-campus
106 transmission. We do not explicitly incorporate vaccination in the current analysis, but our open-
107 access R-code is programmed to facilitate easy extension of our work to include exploration of
108 the varied effects of NPIs on populations with a subset of vaccinated individuals (24), as these
109 scenarios become more pervasive in the 2021 year.

110



111
 112 **Figure 1. Conceptual schematic of branching process model of SARS-CoV-2 dynamics.**
 113 Person A is isolated through testing after exposing Person B and Person C. Person B is then isolated through contact
 114 tracing, while Person C is not traced but is nonetheless ultimately isolated through symptomatic surveillance. A viral
 115 titer trajectory (right) is derived from a within-host viral kinetics model (Supplementary File 1), yielding the mean
 116 titer trajectory and 95% confidence interval shown here. The 25th and 75th titer threshold percentile for the onset of
 117 symptoms are depicted in pink, such that 32% of individuals modeled in our simulations did not present symptoms.
 118 Schematic is adapted in concept from Hellewell et al. (2020) (25).
 119

120
 121 R_E is the product of the pathogen basic reproduction number (R_0) and the proportion of
 122 the population that is susceptible to disease. R_E is thus a dynamic value which corresponds to the
 123 number of new infections caused by a single infection at a given timepoint within a specified
 124 community. We compute an independent R_E for each infectious person in our population that is
 125 the combined result of both heterogeneity in individual infectiousness and heterogeneity in
 126 individual contact events that could result in transmission. To determine R_E , we first draw a
 127 value of potential cases for each infectious individual in our population from the SARS-CoV-2
 128 negative binomial distribution for R_0 , estimated to have a mean value of 2.5 and a dispersion
 129 parameter (k) of 0.10 (26). Though representation of R_E in log-normal vs. negative binomial
 130 form will not change the average number of cases generated per epidemic, the negative binomial
 131 distribution replicates the dynamics of superspreading events, which are known to play an
 132 important role in SARS-CoV-2 dynamics (27–32). Indeed, there is growing direct empirical
 133 evidence that COVID-19 epidemiology exhibits a negative binomial R_E across multiple systems
 134 (31, 33–35); as few as 10% of infectious individuals may be responsible for 80% of onward
 135 SARS-CoV-2 transmissions (36).

136 We next assume that a minority (10%) of possible onward transmissions are lost to the
 137 external community (e.g. an infectious UC Berkeley community member infects someone
 138 outside the UC Berkeley community), and we remove these from our model, such that we
 139 ultimately aim to report within-campus R_E as the number of onward cases that a single infectious
 140 university community member causes within the university community (Supplementary File 1).
 141 To achieve this, we next assume that social distancing, masking, and behavioral modifications in
 142 our community will modulate dynamics such that some of the remaining 90% of the original R_0 -

143 derived potential infections do not take place. Because we are specifically interested in advising
144 UC Berkeley on group size limits for gatherings, we next draw a number of possible onward
145 transmission events for each infectious individual from a simple Poisson distribution with $\lambda = 3$,
146 signifying the average number of possible encounters (i.e. cross-household dining, shared car
147 rides, indoor meetings, etc.) per person that could result in transmission. We then use published
148 estimates of the generation time of onward transmission events for SARS-CoV-2 infection (2) to
149 draw event times for these encounters, and we distribute each infectious person's original
150 number of R_0 -derived potential cases among these events at random. This ensures that multiple
151 transmissions are possible at a single event; the most extreme superspreading events occur when
152 persons with heterogeneously high infectiousness draw a large number of potential cases, which
153 are concentrated within a relatively small number of discrete transmission events. When group
154 size limit NPIs are imposed, case numbers for each event are truncated at the intervention limit.

155 For each infectious individual, we additionally generate an independent virus trajectory,
156 using a within-host viral kinetics model for SARS-CoV-2 upper respiratory tract infections,
157 which is structured after the classic target cell model (37–40). From each independent virus
158 trajectory, we can then infer a time-varying transmissibility, which is modeled as a Michaelis-
159 Menten-like function of viral load (40). Deviating from the original published model, we fix the
160 within-host viral kinetics model constant, θ , at a value that allows for a ~50% probability of
161 infection occurring per transmissible contact event at an infectious individual's peak viral load
162 (40). Because all possible onward transmissions have been assigned an event generation time, we
163 next evaluate the viral load of the infectious person at the time of each potential transmission to
164 determine whether or not it actually takes place. By these metrics, our original R_0 -derived
165 possible cases are halved, such that R_E , the number of average onward infections caused by a
166 single infectious person in the UC Berkeley community, is reduced to just over one ($R_E=1.05$),
167 consistent with published estimates of Bay Area R_E and initial asymptomatic test results in our
168 community (22, 41). The majority of transmission events occur when the infectious host has
169 higher viral titers, thus biasing new case generations towards earlier timesteps in an individual's
170 infection trajectory, as is realistic for COVID-19 (23) (Figure 1).

171 In addition to modulating the probability of onward transmission events, each infectious
172 individual's virus trajectory additionally allows us to compute a timing of symptom onset, which
173 corresponds to the timepoint at which an individual's virus trajectory crosses some threshold
174 value for presentation of symptoms. We draw each threshold randomly from a log-normal
175 distribution with a mean of 10^5 virus copies per μl of RNA; by these metrics, roughly 32% of our
176 modeled population presents as asymptomatic, in keeping with published estimates for SARS-
177 CoV-2 (6, 7). Using each infectious individual's viral load trajectory, we are next able to
178 compute a period of test sensitivity, corresponding to the time during which viral load is high
179 enough for detection by the virus test in question, based on the modeled limit of detection
180 (LOD). Surveillance testing results in higher “false-negative” test results both very early and
181 very late in infection when viral loads are below the LOD for the adopted assay (42) (Figure 1),
182 though most tests should reliably detect infectious cases with viral titers $>10^6$ cp/ μl (43–45). We

183 explore dynamics across a range of published values for test LOD: 10^1 , 10^3 , and 10^5 virus copies
184 per μl of RNA. The IGI's RT-qPCR-based testing pipeline has a published sensitivity of 1 cp/ μl
185 (21), while the majority of SARS-CoV-2 RT-qPCR tests nationally are reliable above a 10^3 cp/ μl
186 threshold (46); less-sensitive antigen-based and LAMP assays report detection limits around 10^5
187 cp/ μl (47, 48).

188 In addition to within-community transmissions, all individuals in the modeled population
189 are also subjected to a daily hazard (0.15%) of becoming infected from an external source, based
190 on published estimates of R_E and COVID-19 prevalence in Alameda County (41, 49). We report
191 the mean results of 100 stochastic runs of each proposed intervention.

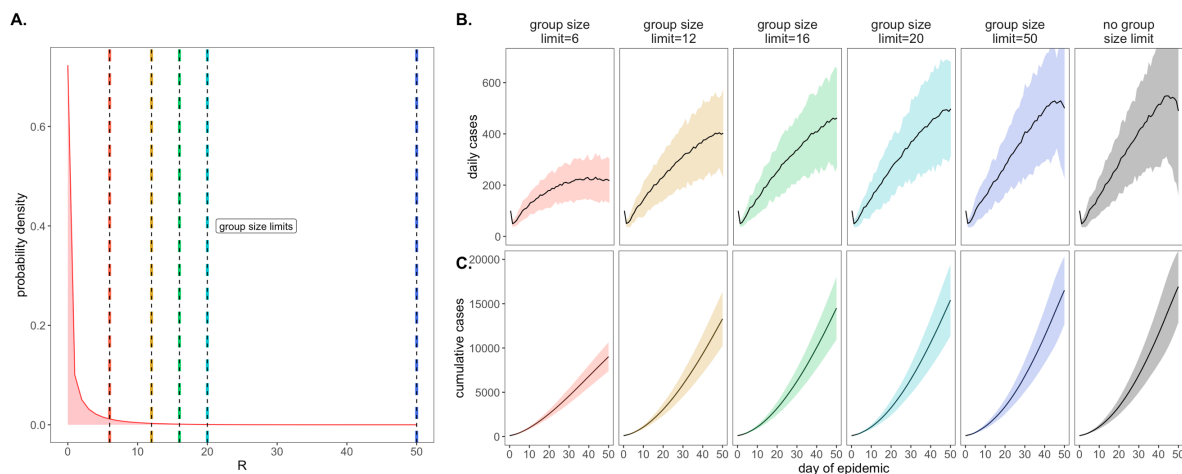
192

193 **Results.**

194 **Comparing behavioral NPIs for COVID-19 control.**

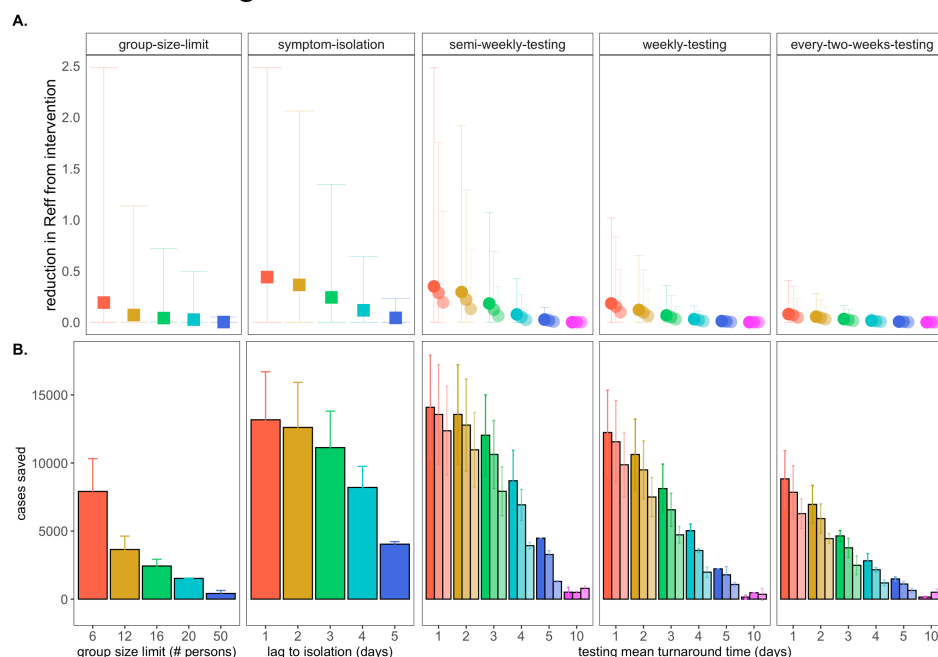
195 We first ran a series of epidemic simulations using a completely mixed population of
196 20,000 individuals subject to the infection dynamics outlined above to compare and contrast the
197 impacts of our four NPIs on COVID-19 control. We introduced an initial population of 100
198 infectious individuals (0.5%) at timestep 0 and compared the effects of a single target
199 intervention on epidemic trajectories after the first 50 days of simulation. Less intensive or
200 intervention-absent scenarios allowed infectious cases to grow at unimpeded exponential rates,
201 rapidly exhausting our susceptible supply and making it necessary to compare results at a
202 consistent (and early) timepoint in our simulated epidemics.

203 As a consequence of our representation of R_E in negative binomial form, we first
204 considered the COVID-19 control effectiveness of group size limits on in-person gatherings,
205 which doubled as upper thresholds in transmission capacity (Figure 2). Assuming that 90% of
206 the modeled population adhered to assumed group size regulations, we found that limiting
207 outdoor gatherings to groups of six or fewer individuals saved a mean of $\sim 7,900$ cases per 50-
208 day simulation (in a 20,000 person population) and corresponded to an R_E reduction of nearly
209 0.20 (reducing R_E from 1.05 to subclinical 0.86; Figure 2; Supplementary File 2). By contrast, a
210 large group size limit of 50 persons had almost no effect on epidemic dynamics; under published
211 estimates of SARS-CoV-2 negative binomial R_E (26), a group size limit of 50 will restrict
212 transmission from only 0.00039% of infectious individuals (Figure 2). Gains in epidemic control
213 from group size limits resulted from avoidance of superspreading events, an approach that was
214 effective for negative binomial but not log-normal representations of R_E that lack the
215 transmission "tail" characteristic of a superspreader distribution (32) (Figure 2-S1). Importantly,
216 by avoiding superspreading events, group size limits also reduced variance in daily case counts,
217 yielding more predictable epidemics, which are easier to control through testing and contact
218 tracing (2, 23, 25). Over the July 4 weekend, surveillance testing resources in our UC Berkeley
219 community were overwhelmed and containment efforts challenged after a single superspreading
220 event on campus (50).



221
 222 **Figure 2. Effects of group size limits on COVID-19 dynamics.**
 223 **A.** Negative binomial R_E distribution with mean = 1.05 and dispersion parameter (k) = 0.10. The colored vertical
 224 dashes indicate group size limits that ‘chop the tail’ on the R_E distribution; for 90% of the population, coincident
 225 cases allocated to the same transmission event were truncated at the corresponding threshold for each intervention.
 226 **B.** Daily new cases and, **C.** Cumulative cases, across a 50-day time series under corresponding, color-coded group
 227 size limits.
 228

229 We next investigated the impacts of variation in lag time to self-isolation post-symptom
 230 onset for the just under 70% of individuals likely to present with COVID-19 symptoms in our
 231 modeled population (Figure 3). At UC Berkeley, all essential students, faculty, and staff must
 232 complete a digital ‘Daily Symptom Screener’ before being cleared to work on campus; here, we
 233 effectively model the delay post-initial symptom onset to the time at which each individual
 234 recognizes symptoms sufficiently to report to the Screener and isolate. For each infected
 235 individual in our population, we draw a symptom-based isolation lag from a log-normal
 236 distribution centered on a mean of one to five days, assuming the entire population to be
 237 compliant with the selected lag.



239 **Figure 3. Impacts of NPIs on COVID-19 control.**

240 **A.** Mean reduction in R_E^* and **B.** cumulative cases saved across 50-day simulated epidemics under assumptions of
241 differing non-pharmacological interventions (NPIs). NPIs are color-coded by threshold number of persons for
242 group-size limits, lag-time for symptom-based isolations, and mean turnaround time from test positivity to isolation
243 of infectious individuals for testing isolations. For testing isolations, shading hue corresponds to test limit of
244 detection (LOD) with the darkest colors indicating the most sensitive tests with an LOD of 10^1 virus copies/ μ l of
245 RNA. Progressively lighter shading corresponds to LOD = 10^3 , 10^5 , and 10^7 cp/ μ l.

246 **Note: R_E reduction (panel A) is calculated as the difference in mean R_E in the absence vs. presence of a given NPI.*
247 *The upper confidence limit (uci) in R_E reduction is calculated as the difference in uci R_E in the absence vs. presence*
248 *of NPI. In our model, mean R_E in the absence of NPI equals 1.05 and uci R_E in the absence of NPI equals 8.6.*

249

250 By these metrics, a rapid, one day lag in symptom-based isolation is the fourth-most
251 effective intervention in our study, with a mean of more than 13,100 cases saved in a 50-day
252 simulation (again, in a 20,000 person population), corresponding to an R_E reduction of 0.67,
253 from 1 to 0.38 (Supplementary File 2). Longer lag times to isolation produced less dramatic
254 results, but even an average five-day lag to isolation post-symptom onset nonetheless yielded
255 more than 4,000 cases saved and reduced R_E by a mean of 0.06. The efficacy of symptom-based
256 isolation decreased at higher virus titer thresholds for symptom onset, corresponding to a higher
257 asymptomatic proportion (~50%) of the population (Figure 3-S1); some empirical findings
258 suggest that these higher titer thresholds for symptom onset may more accurately reflect
259 COVID-19 epidemiology (51). Because both group size limits and daily screening surveys to
260 facilitate symptom-based isolation can be implemented without expending substantial resources,
261 we advocate for these two approaches as particularly cost-effective COVID-19 control strategies
262 for all university and small community environments—especially those lacking an on-site
263 surveillance testing lab.

264

265 **Comparing surveillance testing NPIs for COVID-19 control.**

266 Our primary motivation in developing this model was to advise UC Berkeley on best-
267 practices for asymptomatic surveillance testing. As such, we focused efforts on determining the
268 most effective use of testing resources by comparing surveillance testing across a range of
269 approaches that varied test frequency, test turnaround time (TAT, the time from which the test
270 was administered to the timing of positive case isolation), and test sensitivity (based on the
271 LOD).

272 We compared all permutations of surveillance testing NPIs, varying test frequency across
273 semi-weekly, weekly, and every-two-week regimes, investigating TAT across delays of one to
274 five and ten days, and exploring LODs of 10^1 , 10^3 , and 10^5 virus copies per μ l of RNA. These
275 test frequency regimes reflect those under consideration at UC Berkeley today: from August-
276 December 2020, UC Berkeley undergraduates residing in university residence halls were subject
277 to compulsory semi-weekly asymptomatic surveillance testing, while all other campus
278 community members were permitted to take part in voluntary testing with a recommended
279 weekly or every-two-week frequency. TAT values in our model reflect the reality in range of
280 testing turnaround times from in-house university labs like that at UC Berkeley to institutions

281 forced to outsource testing to commercial suppliers (52), and LOD values span the range in
282 sensitivity of available SARS-CoV-2 tests (21, 46–48).

283 Across testing regimes broadly, we found test frequency, followed by TAT, to be the
284 most effective NPIs, with LOD exerting substantially less influence on epidemic dynamics,
285 consistent with findings published elsewhere (14, 15). The top three most effective NPIs in our
286 study corresponded to semi-weekly testing regimes with one- and two-day TATs across 10^1 and
287 10^3 cp/μl LODs. These three scenarios yielded mean cases saved ranging from just over 14,000
288 to just over 13,500 in the first 50 days of simulation and produced an R_E reduction capacity
289 between 0.97 and 0.80 (Figure 3; Supplementary File 2). Halving test frequency to a weekly
290 regimen, under assumptions of TAT=1 and LOD= 10^1 , resulted in a nearly 48% decrease in the
291 NPI's R_E reduction capacity. By comparison, a single extra day lag from one to two-day TAT
292 under semi-weekly testing conditions at LOD= 10^1 cp/μl yielded a modest 16% decrease in R_E
293 reduction capacity. However, longer delays in TAT of up to ten days or more—not unusual in
294 the early stages of the COVID-19 pandemic (52)—were not significantly different from
295 scenarios in which no intervention was applied at all. This outcome results from the rapid
296 generation time of SARS-CoV-2 (2); most infectious individuals will have already completed the
297 majority of subsequent transmissions by the time a testing isolation with a 10-day TAT is
298 implemented. Nonetheless, encouragingly, reducing test sensitivity from 10^1 to 10^3 under a semi-
299 weekly, TAT=1 regime decreased R_E reduction capacity by only 18%, offering support to
300 advocates for more frequent but less sensitive tests (53) but also highlighting the added benefit
301 incurred when university testing labs, like that at UC Berkeley, are able to provide both frequent
302 and sensitive PCR-based testing.

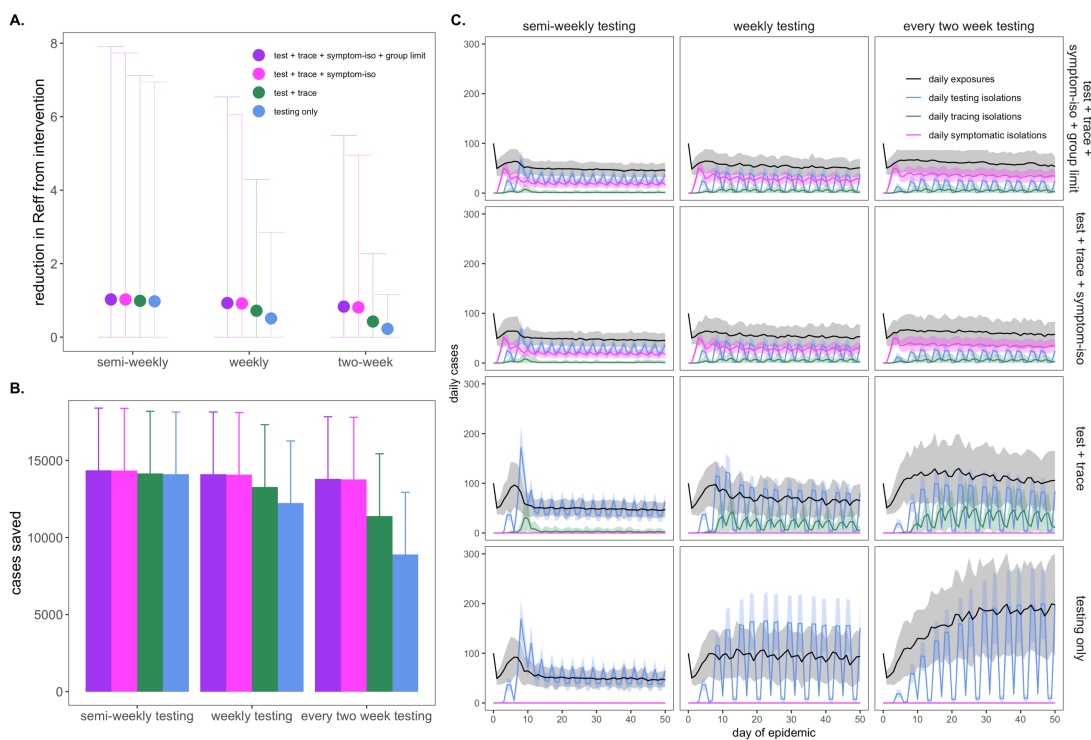
303 Addition of a contact tracing intervention, in which 90% of infectious contacts were
304 traced and isolated within a day of the source host isolation, to NPI scenarios already featuring
305 either symptom-based or surveillance testing isolation enhanced each intervention's capacity for
306 epidemic control (Figure 3-S2). Of note, contact tracing boosted performance of some of the
307 poorest performing testing interventions, such that even those previously ineffective surveillance
308 regimens with 10-day TAT nonetheless averted cases and significantly reduced R_E when
309 infectious contacts could be isolated. For a semi-weekly testing regime at LOD= 10^1 cp/μl and
310 TAT=10 days, the addition of contact tracing increased mean cases saved from ~510 to >8,600
311 and increased R_E reduction capacity from 0.000080 to 0.27 (Supplementary File 3).

312

313 **Optimizing combined NPIs for COVID-19 control.**

314 Our modeled simulations indicate that it is possible to achieve largely equivalent gains in
315 COVID-19 control from NPIs in the form of group size limits, symptom-based isolations, and
316 surveillance testing isolations—though gains from symptom-based behavioral isolations are
317 jeopardized under assumptions of a higher proportion of asymptomatic individuals (Figure 3-S1).
318 Nonetheless, the most effective interventions are realized when behavioral control mechanisms
319 are *combined* with surveillance testing (Figure 4). Assuming a one day TAT and 10^1 cp/μl LOD,
320 we found that adding (a) contact tracing with 90% adherence and a one-day lag, plus (b)

321 symptom-based isolation with a one-day lag, plus (c) a group size limit of twelve persons to an
 322 every-two-week surveillance testing regimen could elevate the R_E reduction capacity from 0.22
 323 to 0.83 and almost double the ~6,600 cases saved from the testing intervention alone
 324 (Supplementary File 4). Combining interventions enables less rigorous testing regimes to rival
 325 the effectiveness of semi-weekly surveillance testing without expending additional resources. In
 326 addition, combining interventions results in less variation in the cumulative case count, as many
 327 layers of opportunity for infection isolation help limit the likelihood of a superspreading event
 328 spiraling out of control (Figure 4-S1).
 329

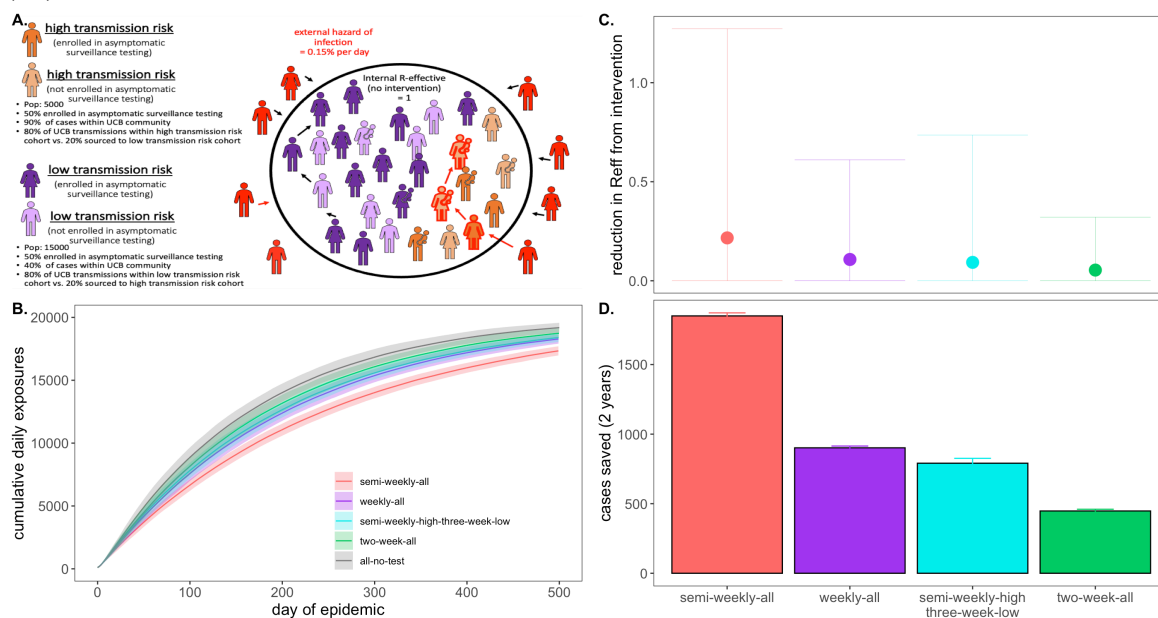


330
 331 **Figure 4. Combining behavioral and surveillance testing NPIs for COVID-19 control.**
 332 **A.** Mean reduction in R_E , **B.** cumulative cases saved, and **C.** daily case counts for the first 50 days of the epidemic,
 333 across regimes of differing testing frequency and a combination of surveillance testing, contact tracing, symptomatic
 334 isolation, and group size limit interventions. All scenarios depicted here assumed test TAT, symptomatic isolation
 335 lags, and contact tracing lags drawn from a log-normal distribution with mean=1. LOD was fixed at 10^1 and group
 336 size limits at 12. Dynamics shown here are from biweekly testing simulations in which testing was limited to two
 337 test days per week.
 338

339 Following on this theme, we also experimented with varying the distribution of days
 340 allocated to surveillance testing, without changing the frequency with which each individual was
 341 tested. Specifically, we explored semi-weekly, weekly, and every-two-week testing regimens in
 342 which tests were administered across two, five, and seven available testing days per week. More
 343 broadly distributed test days corresponded to fewer tests per day at a population level but, as
 344 with more intervention layers, resulted in less variation in the cumulative total cases because
 345 testing isolations more closely tracked daily exposures (Figure 4-S1).
 346

347 **Modeling COVID-19 dynamics in the campus community.**

348 In our final analysis, we sought to advise the IGI on surveillance testing strategies
 349 explicitly by simulating epidemics in a more realistic, heterogeneous population modeled after
 350 the UC Berkeley campus community (Figure 5). To this end, we subdivided our 20,000 person
 351 university population into a 5,000 person “high transmission risk” cohort and a 15,000 person
 352 “low transmission risk” cohort, assuming “high transmission risk” status to correspond to
 353 individuals (such as undergraduates), living in high density housing with a majority of contacts
 354 (90%) concentrated within the UCB community and “low transmission risk status” to correspond
 355 to individuals (such as faculty members or postdoctoral scholars) with only limited contacts
 356 (40%) in the UCB community. We imposed a 12-person group size limit (with 90% adherence)
 357 on the population as a whole, as recommended by the City of Berkeley Public Health
 358 Department in the early months of the pandemic (54), and assumed a one-day average lag in
 359 symptom-based isolation for all cohorts. To add additional realism, we enrolled only 50% of
 360 each transmission risk group in our modeled surveillance testing program (to mimic adherence—
 361 though surveillance testing is compulsory for undergraduates residing in residence halls at UC
 362 Berkeley (22)). We assumed that 95% efficacy in contact tracing (with a mean tracing delay of
 363 one day) for those enrolled in our surveillance program but only 50% efficacy for those not
 364 enrolled; UC Berkeley has encouraged all community members to enroll in the ‘CA Notify’
 365 digital contact tracing app developed by Apple and Google (55). For all testing interventions,
 366 we assumed $LOD=10^1$ cp/ μ l and $TAT=2$ days, the average for the IGI surveillance testing lab
 367 (21).



368
 369
 370
 371
 372
 373
 374

Figure 5. Targeted testing of high transmission risk cohorts in a heterogenous population.

A. Schematic of transmission risk group cohorts in the heterogenous model. The population is divided into 5,000 “high transmission risk” and 15,000 “low transmission risk” individuals, for which, 90% and 40% of the proportion of transmission events take place within the UC Berkeley community, respectively. Of those transmission events within the Berkeley community, the majority (80%) are restricted within the same transmission risk group as the infector, while 20% are sourced to the opposing risk group. Half of each cohort is assumed to be enrolled in

375 asymptomatic surveillance testing and subjected to the differing test frequency regimes depicted in panels **B.**
376 through **D.** Panel **B.** shows the progression of cumulative cases across 730 days of simulation for each testing
377 regime, while panel **C.** and **D.** give, respectively, the reduction in R_E and the total cases saved achieved by each test
378 regime vs. a no intervention baseline.

379
380 We found that targeted, semi-weekly testing of 50% of individuals in the high
381 transmission risk cohort, paired with every-three-week testing of enrolled individuals in the low
382 transmission risk cohort yielded mean R_E reduction and cumulative cases saved on par with that
383 achieved from weekly testing (and better than that achieved from every-two-week testing) of all
384 enrolled individuals in the population at large (Figure 5). Targeting the highest transmission-risk
385 populations with testing surveillance allows practitioners to save valuable testing resources while
386 simultaneously controlling the epidemic for the entire community. Importantly, while mean R_E
387 reduction and cumulative cases were largely comparable between the targeted, semi-weekly
388 testing regiment and the untargeted, weekly regimen, the observed variance in intervention
389 efficacy (Figure 5C) was substantially greater for the targeted scenario, in which the low
390 transmission risk cohort was only tested once every three weeks. This results from a higher
391 probability that a rare superspreading event could occur in the infrequently monitored low
392 transmission risk cohort, thus reaffirming our previous observation that more frequent
393 surveillance testing regimens result in more predictable—and easier to control—epidemics.

394 Notably, irrespective of intervention, the diminished transmissibility of the “low
395 transmission risk” population in this heterogeneous model structure greatly reduced epidemic
396 spread in subsequent simulations as compared with those presented previously in the perfectly
397 mixed environment; as a result, we here compared interventions after 500 days of simulation,
398 rather than 50. The heightened realism of our heterogenous population generated slow-moving
399 epidemics more closely resembling those we are currently witnessing in our university
400 environment.

401 402 **Discussion.**

403 We built a stochastic branching process model of SARS-CoV-2 spread in a university
404 environment to advise UC Berkeley on best-practice strategies for effective asymptomatic
405 surveillance in our pop-up IGI testing lab—and to offer a model for other institutions attempting
406 to control the COVID-19 epidemic in their communities. While previous work has explored the
407 isolated effects of specific NPIs—including group association limits (32), symptomatic isolation
408 (2, 14–16, 23, 25), asymptomatic surveillance testing (14–16), and contact tracing (2, 23, 25)—
409 on COVID-19 control, ours is the only model to date which investigates these interventions
410 simultaneously and does so in a realistic and easily applicable setting. We offer an easy-to-
411 implement modeling tool that can be applied in other educational and workplace settings to
412 provide NPI recommendations tailored to the COVID-19 epidemiology of a specific
413 environment.

414 Results from our analysis of behavior-based NPIs support previous work (2, 14–16, 23,
415 25, 32) in showing that stringent group size limitations to minimize superspreading events and

416 rapid symptom-based isolations offer an effective means of epidemic control in the absence of
417 surveillance testing resources. However, because of the unique natural history of the SARS-
418 CoV-2 virus, for which the majority of transmission events result from asymptomatic or
419 presymptomatic infections (2, 25), symptom-based NPIs cannot reduce epidemic spread
420 completely, and small community environments will always remain vulnerable to asymptomatic
421 case importation. Moreover, symptom-based NPIs pose less effective means of epidemic control
422 under scenarios assuming a higher proportion of asymptomatic individuals; empirical evidence
423 suggests that SARS-CoV-2 infection may result in asymptomatic infection in up to nearly 70%
424 of the population in select environments (51). For this reason, our results emphasize the
425 importance of asymptomatic surveillance testing to prevent ongoing epidemics in universities
426 and other small community environments. As more data becomes available on both the
427 proportion of asymptomatic infections and their contributions to SARS-CoV-2 transmission, the
428 relative importance of group size interventions, symptom-based isolation, and asymptomatic
429 surveillance testing in different epidemiological contexts will be possible to determine from our
430 modeling framework.

431 As with behavioral interventions, our exploration of optimal surveillance testing regimes
432 supports findings that have been published previously but with a few key extensions and critical
433 novel insights. As has been recently highlighted (14, 15), we find that the most cases are saved
434 under asymptomatic testing regimes that prioritize heightened test frequency and rapid
435 turnaround time over test sensitivity. Importantly, we extend previous work to highlight how
436 more rigorous testing regimes—and those combined with one or more behavioral
437 interventions—greatly reduce variance in daily case counts, leading to more predictable
438 epidemics. We find that the reduction in daily case variation is even more pronounced when test
439 regimes of equivalent frequency are distributed more broadly in time (i.e. tests are offered across
440 more days of the week), thus minimizing the likelihood of compounding transmission chains that
441 may follow upon a superspreading event. Additionally, we demonstrate how a focused stringent
442 testing regime for a subset of “high transmission risk” individuals can effectively control a
443 COVID-19 epidemic for the broader community. Taken together, our model shows the utility of
444 a multi-faceted approach to COVID-19 control and offers a flexible tool to aid in prioritization of
445 interventions in different university or workplace settings.

446 Finally, our paper presents the only COVID-19 surveillance model published to date that
447 combines asymptomatic testing with contact tracing, thus highlighting the compounding gains
448 effected by these two interventions: contact tracing amplifies the control impacts of both
449 symptom-based and surveillance testing-based isolations, such that even intervention scenarios
450 assuming long delays in isolation after symptom onset or slow turnaround-times for test results
451 can nonetheless greatly reduce the transmission capacity of COVID-19. These findings further
452 emphasize the critical role that asymptomatic surveillance testing is likely to play in ongoing
453 efforts to control COVID-19 epidemics into the 2021 year. Even limited surveillance testing may
454 offer substantial gains in case reduction for university and workplace settings that already have

455 efficient symptomatic isolation and contact tracing programs in place. Our model allows us to
456 prioritize when and where these gains are most likely to be achieved.

457 Because we do not explicitly model SARS-CoV-2 transmission in a mechanistic,
458 compartmental framework (56, 57), our analysis may overlook some more subtle insights into
459 long-term disease dynamics. More complex analyses of interacting epidemics across larger
460 spatial scales or investigations of vaccination delivery and the duration of immunity will
461 necessitate implementation of a complete compartmental transmission model. However, our use
462 of a stochastic branching process framework makes our model simple to implement and easily
463 transferrable to other semi-contained small community environments, including a wide range of
464 academic settings and workplaces (24). We make this tool available to others interested in
465 exploring the impacts of targeted public health interventions—in particular, surveillance testing
466 regimes—on COVID-19 control in more specific settings in the upcoming 2021 year. We at the
467 University of California, Berkeley are committed to maintaining the safest campus environment
468 possible for our community, using all intervention tools at our disposal. We advise those in
469 similar positions at other institutions to employ the behavioral interventions outlined here, in
470 concert with effective surveillance testing regimes, to reduce community epidemics of COVID-
471 19 in the upcoming spring season.

472

473

474

475 **Acknowledgments and Funding Sources**

476 CEB was funded by the Miller Institute for Basic Research at the University of California,
477 Berkeley, the Branco Weiss Society in Science Fellowship from ETH Zurich, a DARPA
478 PREEMPT Cooperative Grant (no. D18AC00031), and a COVID-19 Rapid Response Research
479 grant from the Innovative Genomics Institute at the University of California, Berkeley. MB was
480 supported by NIH grant no. R01-GM122061-03 and NSF EEID grant no. 2011109.

481

482

483

484

485

486

487

488

489

490

491

492

493

494

495 **References**

- 496 1. Fraser C, Riley S, Anderson RM, Ferguson NM (2004) Factors that make an infectious
497 disease outbreak controllable. *Proc Natl Acad Sci U S A* 101(16):6146–6151.
- 498 2. Ferretti L, et al. (2020) Quantifying SARS-CoV-2 transmission suggests epidemic control
499 with digital contact tracing. *Science* 368(6491):eabb6936.
- 500 3. Petersen E, et al. (2020) Comparing SARS-CoV-2 with SARS-CoV and influenza
501 pandemics. *Lancet Infect Dis* 20(9):e238–e244.
- 502 4. WHO (2020) Coronavirus disease (COVID-2019) situation reports. Available at:
503 <https://www.who.int/emergencies/diseases/novel-coronavirus-2019/situation-reports>
504 [Accessed June 30, 2020].
- 505 5. Oran DP, Topol EJ (2020) Prevalence of asymptomatic SARS-CoV-2 infection: A
506 narrative review. *Ann Intern Med* 173(5):362–367.
- 507 6. Mizumoto K, Kagaya K, Zarebski A, Chowell G (2020) Estimating the asymptomatic
508 proportion of coronavirus disease 2019 (COVID-19) cases on board the Diamond Princess
509 cruise ship, Yokohama, Japan, 2020. *Eurosurveillance* 25(10):1–5.
- 510 7. Nishiura H, et al. (2020) Estimation of the asymptomatic ratio of novel coronavirus
511 infections (COVID-19). *Int J Infect Dis* 94:154–155.
- 512 8. Treibel TA, et al. (2020) COVID-19: PCR screening of asymptomatic health-care workers
513 at London hospital. *Lancet* 395(10237):1608–1610.
- 514 9. Emery JC, et al. (2020) The contribution of asymptomatic SARS-CoV-2 infections to
515 transmission on the Diamond Princess cruise ship. *Elife* 9:1–68.
- 516 10. Gandhi M, Yokoe DS, Havlir D V. (2020) Asymptomatic transmission, the achilles’ heel
517 of current strategies to control COVID-19. *N Engl J Med* 382(22):2158–2160.
- 518 11. Boyles S (2020) Covid-19: Asymptomatic transmission fueled nursing home death toll.
519 *Physicians’ Wkly*.
- 520 12. Kam KQ, et al. (2020) A well infant with Coronavirus Disease 2019 (COVID-19) with
521 high viral load. *Clin Infect Dis*:ciaa201.
- 522 13. Bai T, et al. (2020) Presumed asymptomatic carrier transmission of COVID-19. *J Am Med*
523 *Assoc* 382(13):1199–1207.
- 524 14. Larremore DB, et al. (2020) Test sensitivity is secondary to frequency and turnaround
525 time for COVID-19 surveillance. *bioRxiv*:1–21.
- 526 15. Bergstrom T, Bergstrom CT, Li H (2020) Frequency and accuracy of proactive testing for
527 COVID-19. *medRxiv*:2020.09.05.20188839.
- 528 16. Paltiel AD, Zheng A, Walensky RP (2020) Assessment of SARS-CoV-2 Screening
529 Strategies to Permit the Safe Reopening of College Campuses in the United States. *JAMA*
530 *Netw open* 3(7):e2016818.
- 531 17. Hubler S, Hartocollis A (2020) How Colleges Became the New Covid Hot Spots. *New*
532 *York Times*.
- 533 18. Richtel M (2020) Looking to Reopen, Colleges Become Labs for Coronavirus Tests and
534 Tracking Apps. *New York Times*.

- 535 19. Nietzel MT (2020) As Covid-19 Lingers On, Universities Are Adjusting Their Spring
536 Semester Plans, Often Eliminating Spring Break. *Forbes*.
- 537 20. Ghebreyesus TA (2020) WHO director-general's opening remarks at the media briefing
538 on COVID-19. Available at: [https://www.who.int/dg/speeches/detail/who-director-](https://www.who.int/dg/speeches/detail/who-director-general-s-opening-remarks-at-the-media-briefing-on-covid-19---11-march-2020)
539 [general-s-opening-remarks-at-the-media-briefing-on-covid-19---11-march-2020](https://www.who.int/dg/speeches/detail/who-director-general-s-opening-remarks-at-the-media-briefing-on-covid-19---11-march-2020).
- 540 21. Amen AM, et al. (2020) Blueprint for a pop-up SARS-CoV-2 testing lab. *Nat Biotechnol*
541 (March). doi:10.1038/s41587-020-0583-3.
- 542 22. UC Berkeley COVID-19 Dashboard Available at:
543 [https://coronavirus.berkeley.edu/dashboard/?utm_source=Response+and+Recovery&utm_](https://coronavirus.berkeley.edu/dashboard/?utm_source=Response+and+Recovery&utm_campaign=5247da06c4-Response_Recovery_2020_10_09&utm_medium=email&utm_term=0_940930e328-5247da06c4-389116456)
544 [campaign=5247da06c4-](https://coronavirus.berkeley.edu/dashboard/?utm_source=Response+and+Recovery&utm_campaign=5247da06c4-Response_Recovery_2020_10_09&utm_medium=email&utm_term=0_940930e328-5247da06c4-389116456)
545 [Response_Recovery_2020_10_09&utm_medium=email&utm_term=0_940930e328-](https://coronavirus.berkeley.edu/dashboard/?utm_source=Response+and+Recovery&utm_campaign=5247da06c4-Response_Recovery_2020_10_09&utm_medium=email&utm_term=0_940930e328-5247da06c4-389116456)
546 [5247da06c4-389116456](https://coronavirus.berkeley.edu/dashboard/?utm_source=Response+and+Recovery&utm_campaign=5247da06c4-Response_Recovery_2020_10_09&utm_medium=email&utm_term=0_940930e328-5247da06c4-389116456) [Accessed October 1, 2020].
- 547 23. Peak CM, et al. (2020) Individual quarantine versus active monitoring of contacts for the
548 mitigation of COVID-19: a modelling study. *Lancet Infect Dis*
549 3099(20):2020.03.05.20031088.
- 550 24. Brook CE, Northrup GR, Boots M (2020) Code for “Optimizing COVID-19 control with
551 asymptomatic surveillance testing in a university environment.”
552 doi:10.5281/zenodo.4131223.
- 553 25. Hellewell J, et al. (2020) Feasibility of controlling COVID-19 outbreaks by isolation of
554 cases and contacts. *Lancet Glob Heal* 8(4):e488–e496.
- 555 26. Endo A, Abbott S, Kucharski AJ, Funk S (2020) Estimating the overdispersion in
556 COVID-19 transmission using outbreak sizes outside China. *Wellcome Open Res* 5:67.
- 557 27. Jumar S, Jha S, Rai SK (2020) Significance of super spreader events in COVID-19. *Indian*
558 *J Public Health* 64(6):139–141.
- 559 28. Althouse BM, et al. (2020) Stochasticity and heterogeneity in the transmission dynamics
560 of SARS-CoV-2. *arXiv* (425):1–10.
- 561 29. Hébert-Dufresne L, Althouse BM, Scarpino S V., Allard A (2020) Beyond R0:
562 Heterogeneity in secondary infections and probabilistic epidemic forecasting. *medRxiv*
563 0(1):1–8.
- 564 30. Liu Y, Eggo RM, Kucharski AJ (2020) Secondary attack rate and superspreading events
565 for SARS-CoV-2. *Lancet* 395(10227):e47.
- 566 31. Adam DC, et al. (2559) Clustering and superspreading potential of severe acute
567 respiratory syndrome coronavirus 2 (SARS-CoV-2) infections in Hong Kong. *J Vis Lang*
568 *Comput* 11(3):55.
- 569 32. Kain MP, Childs ML, Becker AD, Mordecai EA (2020) Chopping the tail: how preventing
570 superspreading can help to maintain COVID-19 control. *medRxiv Prepr Serv Heal Sci*.
571 doi:10.1101/2020.06.30.20143115.
- 572 33. Laxminarayan R, et al. (2020) Epidemiology and transmission dynamics of COVID-19 in
573 two Indian states. *Science* 28(2):eabd7672.
- 574 34. Lau MSY, et al. (2020) Characterizing superspreading events and age-specific
575 infectiousness of SARS-CoV-2 transmission in Georgia, USA. *Proc Natl Acad Sci U S A*
576 117(36):22430–22435.

- 577 35. Goyal A, Reeves DB, Fabian Cardozo-Ojeda E, Schiffer JT, Mayer BT (2020) Wrong
578 person, place and time: viral load and contact network structure predict 4 SARS-CoV-2
579 transmission and super-spreading events 5 6 7. *medRxiv*:2020.08.07.20169920.
- 580 36. Nielsen BF, Sneppen K (2020) COVID-19 superspreading suggests mitigation by social
581 network modulation. *medRxiv*:2020.09.15.20195008.
- 582 37. Perelson AS (2002) Modelling viral and immune system dynamics. *Nat Rev Immunol*
583 2(1):28–36.
- 584 38. Ho DD, et al. (1995) Rapid turnover of plasma virions and CD4 lymphocytes in HIV-1
585 infection. *Nature* 373:123–126.
- 586 39. Nowak MA, May RM (2000) *Virus Dynamics: Mathematical Principles of Immunology*
587 *and Virology* (Oxford University Press, Oxford, UK).
- 588 40. Ke R, Zitzmann C, Ribeiro RM, Perelson AS (2020) Kinetics of SARS-CoV-2 infection in
589 the human upper and lower respiratory tracts and their relationship with infectiousness.
590 *medRxiv*:2020.09.25.20201772.
- 591 41. Schwab J, Balzer LB, Geng E, Peng J, Petersen ML Local Epidemic Modeling for
592 Management and Action. Available at: <https://localepi.github.io/LEMMA/>.
- 593 42. Kucirka LM, Lauer SA, Laeyendecker O, Boon D, Lessler J (2020) Variation in false-
594 negative rate of reverse transcriptase polymerase chain reaction–based SARS-CoV-2 tests
595 by time since exposure. *Ann Intern Med*. doi:10.7326/m20-1495.
- 596 43. Wölfel R, et al. (2020) Virological assessment of hospitalized patients with COVID-2019.
597 *Nature* 581(7809):465–469.
- 598 44. Quicke K, et al. (2020) Longitudinal surveillance for SARS-CoV-2 RNA among
599 asymptomatic staff in five Colorado skilled nursing facilities: Epidemiologic, virologic
600 and sequence analysis. *medRxiv*. doi:10.1101/2020.06.08.20125989v1.
- 601 45. La Scola B, et al. (2020) Viral RNA load as determined by cell culture as a management
602 tool for discharge of SARS-CoV-2 patients from infectious disease wards. *Eur J Clin*
603 *Microbiol Infect Dis* 39(6):1059–1061.
- 604 46. Vogels CBF, et al. (2020) Analytical sensitivity and efficiency comparisons of SARS-
605 CoV-2 RT–qPCR primer–probe sets. *Nat Microbiol* (4). doi:10.1038/s41564-020-0761-6.
- 606 47. Meyerson NR, et al. (2020) A community-deployable SARS-CoV-2 screening test using
607 raw saliva with 45 minutes sample-to-results turnaround. *medRxiv*:2020.07.16.20150250.
- 608 48. Dao Thi VL, et al. (2020) A colorimetric RT-LAMP assay and LAMP-sequencing for
609 detecting SARS-CoV-2 RNA in clinical samples. *Sci Transl Med* 12(556).
610 doi:10.1126/SCITRANSLMED.ABC7075.
- 611 49. Chitwood MH, et al. (2020) Bayesian nowcasting with adjustment for delayed and
612 incomplete reporting to estimate COVID-19 infections in the United States. *medRxiv*
613 20(7):1–6.
- 614 50. Public Affairs UB (2020) Social gatherings produce increase in student COVID-19 cases.
615 *Berkeley News*.
- 616 51. Poletti P, et al. (2020) Probability of symptoms and critical disease after SARS-CoV-2
617 infection. *arXiv*. Available at: <http://arxiv.org/abs/2006.08471>.

618 52. Wu KJ (2020) 'It's Like Groundhog Day': Coronavirus Testing Labs Again Lack Key
619 Supplies. *New York Times*.

620 53. Meyer R, Madrigal AC (2020) The Plan That Could Give Us Our Lives Back. *Atl*.

621 54. Officer C of BPH (2020) *Order of the Health Officer of the City of Berkeley Imposing*
622 *Measure Necessary to Control the Spread of COVID-19*.

623 55. Health USD (2020) CA Notify. Available at: <https://canotify.ca.gov/> [Accessed December
624 21, 2020].

625 56. Anderson RM, May RM, Boily MC, Garnett GP, Rowley JT (1991) The spread of HIV-1
626 in Africa: sexual conflict patterns and the predicted demographic impact of AIDS. *Nature*
627 352:581–589.

628 57. Kermack WO, McKendrick AG (1927) A contribution to the mathematical theory of
629 epidemics. *Proc R Soc London, Ser A* 115:700–721.

630

631

632

633

634

635

636

637

638

639

640

641

642

643

644

645

646

647

648

649

650

651

652

653

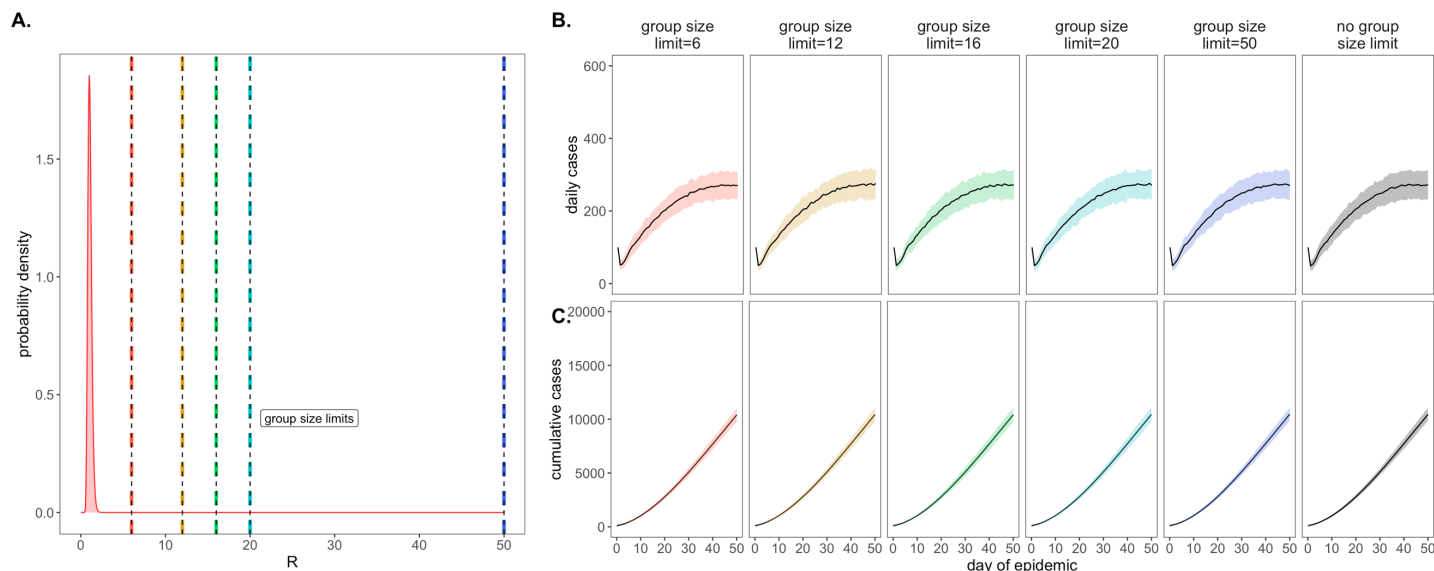
654

655

656

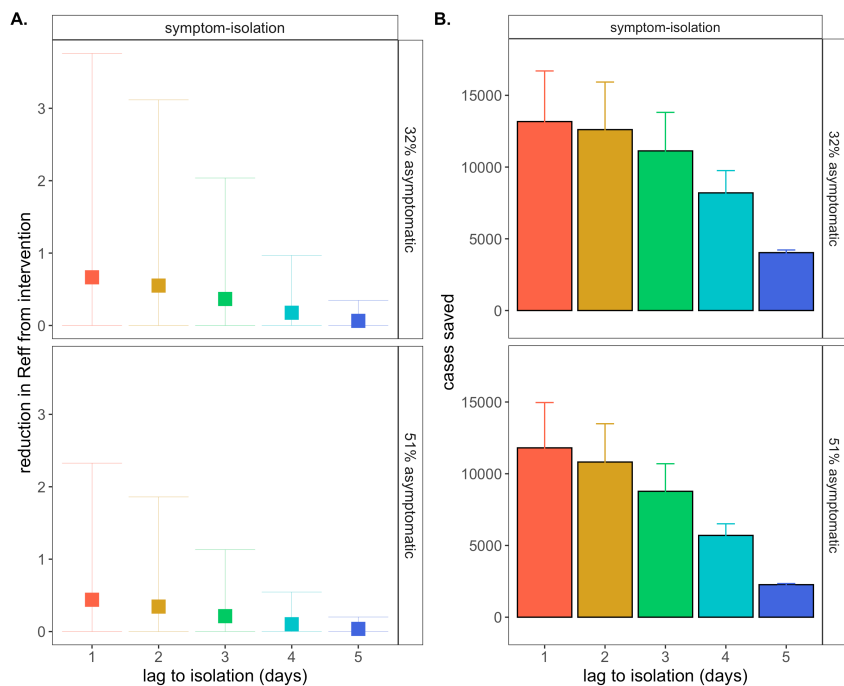
657

658 **Supplementary Figures**
659

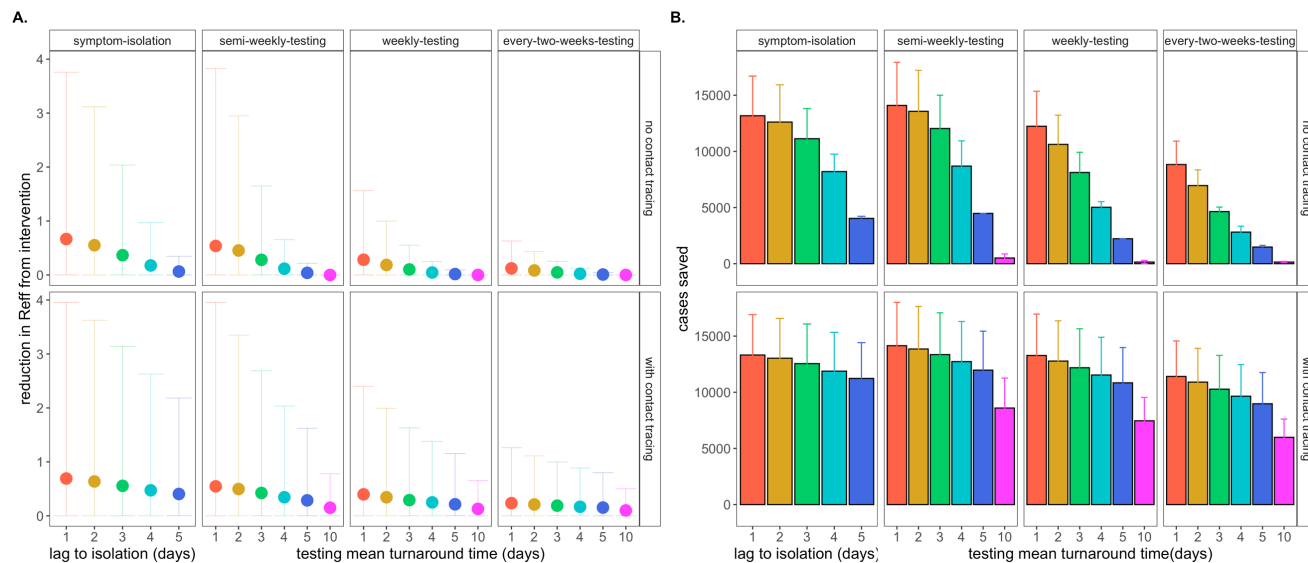


660
661 **Figure 2-S1.** Figure replicates Fig. 2 (main text) at a log-normal distribution for R_E , instead of negative binomial. **A.**
662 Log-normal R_E distribution with a mean of 1.05 and a standard deviation of 1.233. The colored vertical dashes
663 indicate the group size limits that ‘chop the tail’ on the R_E distribution. **B.** Daily new cases and, **C.** cumulative cases,
664 across a 50-day time series under corresponding, color-coded group size limits.

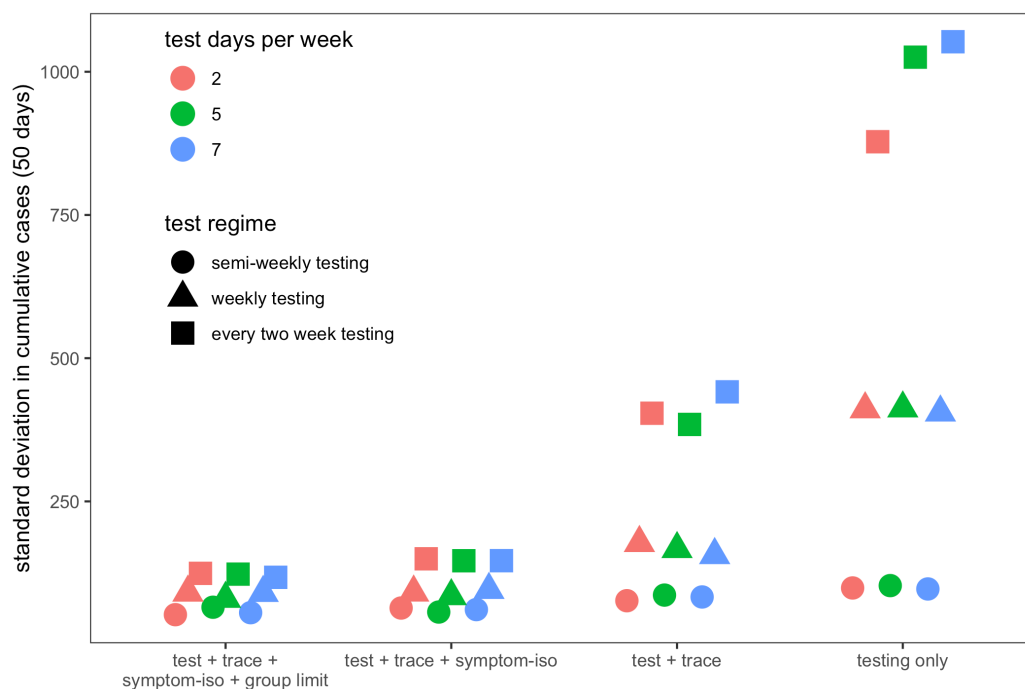
665



666
667 **Figure 3-S1.** Figure replicates symptom-isolation panels from Fig. 3 (main text) in top row, showing **A.** mean
668 reduction in R_E and **B.** cumulative cases saved across 50-day simulated epidemics under differing lag times to
669 isolation, assuming a threshold titer for symptom onset by which ~32% of the population presents as asymptomatic.
670 A comparison at a titer threshold for which ~51% of the population presents as asymptomatic demonstrates how a
671 higher proportion of asymptomatic individuals in the population erodes the effectiveness of the symptom-based
672 isolation intervention; asymptomatic status has no impact on the effectiveness of group size limits or asymptomatic
673 surveillance testing interventions.



674
 675 **Figure 3-S2.** Figure replicates symptom-isolation panels from Fig. 3 (main text) in top row, showing **A.** mean
 676 reduction in R_E and **B.** cumulative cases saved across 50-day simulated epidemics for NPIs of both symptom-based
 677 and testing-based isolation, across a range of different lag times or turnaround times to isolation (for, respectively
 678 symptom- or testing-based isolations). All testing-based interventions depicted are shown at a $LOD=10^1$ cp/ μ l. In
 679 the bottom row, **A.** mean reduction in R_E and **B.** cumulative cases saved are depicted for a comparative intervention
 680 which adds an additional single-day lag in contact tracing to the respective symptom-based or testing-based
 681 isolation. Under these combined interventions, even previously ineffective testing interventions with 10-day TAT
 682 show gains beyond no intervention at all.



683
 684 **Figure 4-S1.** Figure extends results from Fig. 4 (main text), showing the standard deviation in cumulative cases
 685 from 50-day simulated epidemics, across regimes of differing testing frequency and a combination of surveillance
 686 testing, contact tracing, symptomatic isolation, and group size limit interventions. All scenarios depicted here
 687 assume test TAT, symptomatic isolation lags, and contact tracing lags drawn from a log-normal distribution with
 688 mean=1. LOD is fixed at 10^1 and group size limits at 12. Dynamics compare tests of differing frequency (semi-
 689 weekly, weekly, every two weeks) distributed across variable numbers of days in a given week (2,5,7). Additional
 690 layers of intervention and more testing days per week reduce the standard deviation in cumulative cases.

1 **Supplementary File 1.**

2

3 **Text A. *Model Description.***

4 Our publicly-available Github repository (1) provides opensource code to reproduce all
5 simulations and analyses presented in our paper. We summarize the practical implementation
6 details of our modeling design for ease-of-access here.

7 Our model takes the form of a stochastic branching process model, in which a subset
8 population of exposed individuals (0.5%, derived from the mean percentage of positive tests in
9 our UC Berkeley community (2)) is introduced into a hypothetical 20,000 person community that
10 approximates the campus utilization goals for our university in spring 2021. The model code
11 builds up to a single function `replicate.epidemic()` which runs a specified number of stochastic
12 simulations from a defined parameter set, using the function `simulate.epidemic()`. Within the
13 `simulate.epidemic()` function, we first construct a population of 20,000 persons in the sub-
14 function, `initiate.pop()`. Within this initiation function, each person in our population is
15 individually numbered, assigned a viral titer trajectory that will be followed if that individual
16 becomes infected (Text B), and assigned a suite of disease metrics drawn stochastically from a
17 specified set of parameter distributions, as outlined in Text C.

18

19 **Text B. *Within-host viral dynamics***

20 *Titer Trajectories.*

21 For computational efficiency, we pre-generated 20,000 50-day individual titer trajectories
22 and saved them as an .Rdata file, "titer.dat.20K.Rdata". To generate these trajectories, we used
23 a within-host viral kinetics model structured after the classic target cell model (3–5). Code for
24 this model is available in the `model-sandbox` folder of our Github release, under file `viral-
25 load.R`, which iterates the following simple model and parameter values derived from Ke et al.
26 (2020), describing the dynamics of SARS-CoV-2 proliferation in the upper respiratory tract (6):
27

$$28 \frac{dT_C}{dt} = -\beta T_C V$$

$$29 \frac{dE}{dt} = \beta T_C V - kE$$

$$30 \frac{dI}{dt} = kE - \delta I$$

$$31 \frac{dV}{dt} = pI - cV$$

32

33 where T_C corresponds to the target cell population, β is the transmission rate of free virus to
34 target cell invasion, k corresponds to the inverse of the duration of the virus eclipse phase, and δ
35 corresponds to the inverse of the incubation period of an infected cell. p then gives the burst size
36 of a virus-infected cell and c equals the inverse of the lifespan of free virus subject to natural

37 virus mortality and immune predation. Parameter values used to generate each titer trajectory
38 (with a standard deviation of .1x the value of each parameter introduced to add stochasticity in
39 each iteration) are derived from Ke et al. (2020) (6), after fitting this model to individual patient
40 data tracking viral loads through time in the upper respiratory tract of SARS-CoV-2-infected
41 individuals:

42

43 *starting conditions:* $T_C = 4 * 10^6$; $E = 0$; $I = 1$; $V = 0$

44 *parameter values:* $\beta = 1.9 * 10^{-6}$; $k = 4$; $c = 10$; $\delta = 1.9$; $p = 51.4$

45

46 Note that Ke et al. (2020) (6) also explore the within-host dynamics of SARS-CoV-2 infection in
47 the lower respiratory tract; however, since we model human-to-human transmissibility as
48 inferred by viral load in nasopharyngeal swab samples (which better reflect the viral load in the
49 upper respiratory tract), we ignore the lower respiratory dynamics here.

50

51 *Infectivity by Viral Load.*

52 After Ke et al. (2020) (6), we next estimated the probability of infection given contact at a
53 specific viral load, using a Michaelis-Menton-like function. Following Ke et al. (2020), we
54 described the probability this probability as:

55
$$P(\text{transmission}) = 1 - \exp\left(-1 * \left(\theta \left(\frac{V}{V + K_m}\right)\right)\right)$$

56 where K_m corresponds to the saturation constant by which proportional gains in infectiousness
57 with viral load diminish at increasingly high viral titers and θ is a constant, such that the
58 maximum transmission capacity at any moment equals $1 - e^{-\theta}$. Ke et al. (2020) modeled a
59 constant hazard of contact events for infectious individuals and therefore fixed θ at a value of
60 0.05, corresponding to a ~5% probability of a given contact resulting in transmission. Because
61 we draw possible transmissions events from a negative binomial SARS-CoV-2 R_0 distribution,
62 (mean= 2.5 and $k=0.10$ (7)) but ultimately know that R_E for our university environment should
63 have a value of just above one (8), we instead fixed θ at a value of 0.72, corresponding to a
64 ~51% probability of a given contact resulting in transmission, thus effectively halving R_0
65 to generate R_E . The exact probability varied as a function of the timing of each contact event across
66 the trajectory of within-host viral load, with transmissions favored earlier in an infection
67 trajectory when viral load peaks (9).

68

69 **Text C. Individual disease metrics**

70 Figures in our paper are derived from 100x replications of each set of parameter values, which
71 we manipulate to explore a range of non-pharmaceutical interventions (NPIs) to combat COVID-
72 19 dynamics in our system. Our flexible model allows for the introduction of NPIs for COVID-
73 19 control in four different forms: (1) group size limits, (2) symptom-based isolations, (3)
74 surveillance testing isolations, and (4) contact tracing isolations that follow after cases are
75 identified through screening from symptomatic or surveillance testing. These interventions

76 modify the suite of disease metrics drawn upon model initiation for each numbered individual in
77 the dataset. We summarize the disease metrics drawn at initiation for all members of the
78 population here:

- 79 • **Time of next test:** allocated based on the selected asymptomatic surveillance testing regime.
80 We assume the week starts with day 1 on Saturday and day 7 on Friday. If $n.test.days = 2$, then
81 tests are distributed on Monday (day 3) and Friday (day 7) of each week. As timesteps
82 advance and individuals reach their respective test days, the next test day is updated based on
83 the testing regime (if semi-weekly, the next test day is advanced 3 days; if weekly, the next
84 test day is advanced 7 days; if every-two-weeks, the next test day is advanced 14 days).
- 85 • **Beginning/end time of test sensitivity:** based on test limit of detection (LOD) as specified at
86 model outset, this corresponds to the timestep post exposure at which an individual viral titer
87 crosses the threshold for being detectable by the chosen test, both as titers increase at the
88 beginning of a disease trajectory and decrease at the end.
- 89 • **Adherence with testing regime:** Y/N, allocated randomly across individuals based on the
90 proportion of the population modeled as complying with the surveillance testing intervention
91 (90% of individuals in all scenarios modeled in our paper).
- 92 • **Adherence with group limit:** Y/N, allocated randomly across individuals based on the
93 proportion of the population modeled as complying with the group size limits imposed at
94 outset (90% of individuals in all scenarios modeled in our paper; see ‘number of potential
95 onward cases generated for’ for how group size interacts with cases).
- 96 • **Adherence with contact tracing regimen:** Y/N, allocated randomly across individuals based
97 on the proportion of the population modeled as complying with the contact tracing
98 intervention imposed at outset (90% of individuals in all scenarios modeled in our paper).
- 99 • **Time of symptom onset:** determined by randomly drawing a titer limit for symptom onset for
100 each individual from a lognormal distribution with a mean of $1e+05$ cp/ μ l RNA and a
101 standard deviation of $1e+04$ cp/ μ l (10–12). The timing of symptom onset then corresponds to
102 the time post-exposure at which each individual’s titer trajectory crosses the corresponding
103 titer limit. According to this approach, under default parameter values, symptom onset
104 occurred between 2 to 4 days post-exposure in our model, and ~32% of the population never
105 presented with symptoms at all (Fig. 1, main text).
- 106 • **Time of symptom-based isolation:** based on delay lag post-symptom onset, drawn from a
107 lognormal distribution with a mean of the specified number of days of symptom isolation lag
108 (1-5 or infinity) and a standard deviation of 0.5 days.
- 109 • **Time of tracing-based isolation:** based on contact tracing lag for those adhering to the
110 contact tracing regimen in place. Parameter must be updated with each timestep until
111 individual becomes infected; value then becomes fixed at time of infector isolation, plus
112 corresponding lag drawn from a lognormal distribution with a mean of one day and a standard
113 deviation of 0.5 days.

- 114 • **Time of testing-based isolation:** based on turnaround time (TAT) to isolation post testing,
115 drawn from a lognormal distribution with a mean of the specified number of delay days (1-5,
116 10, or infinity) and a standard deviation of 0.5 days. Parameter is updated when ‘time of next
117 test’ is updated for each individual in our model.
- 118 • **Disease status:** ‘susceptible’ = 0, ‘exposed’ = 3, ‘infectious’ = 1, ‘recovered’ = 5. At onset, all
119 individuals are modeled as susceptible, excepting the 0.5% which are introduced as infectious
120 (1) to seed the epidemic. *Note that our model encodes a “prop-vaccinated” parameter for the*
121 *proportion of the target population that is vaccinated prior to the start of epidemic*
122 *simulations. Though we do not explore vaccination scenarios in this analysis, other*
123 *practitioners interested in exploring the efficacy of each NPI on populations with a subset of*
124 *immunized individuals could alter this value (currently fixed at 0) to reflect this. The*
125 *proportion of the population that is specified as vaccinated will then be assigned disease*
126 *status = 5 (recovered) at the onset of each simulation.*
- 127 • **Number of potential onward cases generated:** Several figures in the main text of our
128 manuscript present the R_E reduction capacity of a specified intervention, which we calculate
129 as the difference between the average of the number of potential onward cases generated and
130 the number of actual onward cases generated for each individual after an intervention is
131 adopted. To compute the number of potential onward cases generated for each individual, we
132 first draw a number of possible cases from a negative binomial distribution with a mean of 2.5
133 and a dispersion parameter (k) of 0.10, as estimated for SARS-CoV-2 (7). Next, we draw a
134 number of possible onward transmission events for each infectious individual from a simple
135 Poisson distribution with $\lambda = 3$, signifying the average number of possible encounters (i.e.
136 cross-household dining, shared car rides, indoor meetings, etc.) per person that could result in
137 transmission. We then distribute each infectious person’s original number of R_0 -derived
138 potential cases among these events at random, ensuring that multiple transmissions are
139 possible at a single event; the most extreme superspreading events thus occur when persons
140 with heterogeneously high infectiousness draw a large number of potential cases, which are
141 concentrated within a relatively small number of discrete transmission events. For example, if
142 an infectious individual draws an R_0 value of 16 and an event number value of 4, then those
143 16 potential infections are randomly distributed among 4 events.

144 Next, we use published estimates of the generation time of onward transmission events for
145 SARS-CoV-2 infection to draw event times for each event, based on a weibull distribution
146 with a shape parameter = 2.826 and a scale parameter = 5.665, as specified in Ferretti et al.
147 (2020) (9). Following the above example, 4 discrete generation times would be assigned to
148 cases across the 4 pre-allocated events.

149 Since each individual is already pre-assigned a within-host viral titer trajectory in our
150 modeling framework, we next examine the viral load specified at the generation time of each
151 transmission event and determine if each case assigned to that event actually occurs. Each
152 case is considered individually, and the probability of transmission is computed stochastically
153 based on the value of the individual’s viral titer at the time of the event (higher titer infections

154 are more likely to generate onward transmission events) (Text B). In the above example, all
155 16 possible transmissions would be individually assessed, though several would have the
156 same titer, corresponding to the infectious person's titer at the time point of each contact event
157 (4 possible). Since our maximum probability of a case occurring at max viral load is ~51%
158 (Text B), our original R_0 -derived cases are here halved, resulting in an average of 1.05 onward
159 transmission events per infectious individual in the absence of the NPIs examined here (but
160 reflecting social distancing and mask wearing), which, as specified in the main text, is in line
161 with current estimates from Alameda County, CA (8).

162 For the purposes of our example, let's assume that 10 of those possible 16 cases occur,
163 allocated across 4 different events, with 7 cases at one event and one case each at 3 other
164 events.

165 • **Number of actual onward cases generated:** From the number of possible cases generated,
166 we next apply the relevant intervention and iterate forward in time to determine the actual
167 number of cases generated by each infectious individual across the time course of our
168 modeled epidemics. For symptom and surveillance testing-based isolations, as well as contact
169 tracing, no cases are generated if an infectious individual is isolated prior to the generation
170 time of any possible onward cases. For NPIs in the form of group size limits, case reduction in
171 our model is performed prior to the initiation of the epidemic time series, and case numbers
172 for each transmission event are truncated at the intervention limit.

173 Again following the example listed above, if we imagine that the imposed group size limit
174 is 6, then the 7 cases assigned to a single event will be truncated to 6, meaning that 9 out of
175 the 10 potential cases is allowed to occur after the intervention. Our model is conservative in
176 assessing the impact of a group-size intervention by allowing some portion of those
177 superspreading cases to occur, rather than assuming that a group size limit-abiding infectious
178 individual does not attend larger-than-allowable events altogether. Because only 90% of the
179 population adheres to group size intervention in any given simulation, some proportion of
180 large superspreading events will still take place at random, even after NPIs are imposed.

181
182 Following onset of infection, the timings of symptom-, tracing-, and asymptomatic testing-based
183 isolations are then compared and the earliest time is selected as the actual mechanism (if any) of
184 isolation for that individual. The number of actual onward cases generated is then updated if
185 isolation occurs prior to some new case generations. Additionally, all individuals identified as
186 infectious are additionally assigned the following metrics:

- 187 • **Isolation time of infector**
- 188 • **Source of infection** (external Alameda County vs. UC Berkeley community member)
- 189 • **ID number of infector**, if from UC Berkeley

190 The cycle then repeats in the next timestep when all "actual infections" for each infectious
191 individual are then assigned to new susceptible individuals. The epidemic continues with

192 updated parameters for all newly exposed individuals until either the end of the time series is
193 reached or no more susceptible individuals remain in the population.

194

195 **References for Supplementary File 1.**

- 196 1. Brook CE, Northrup GR, Boots M (2020) Code for “Optimizing COVID-19 control with
197 asymptomatic surveillance testing in a university environment.”
198 doi:10.5281/zenodo.4131223.
- 199 2. UC Berkeley COVID-19 Dashboard Available at:
200 [https://coronavirus.berkeley.edu/dashboard/?utm_source=Response+and+Recovery&utm_](https://coronavirus.berkeley.edu/dashboard/?utm_source=Response+and+Recovery&utm_campaign=5247da06c4-Response_Recovery_2020_10_09&utm_medium=email&utm_term=0_940930e328-5247da06c4-389116456)
201 [campaign=5247da06c4-](https://coronavirus.berkeley.edu/dashboard/?utm_source=Response+and+Recovery&utm_campaign=5247da06c4-Response_Recovery_2020_10_09&utm_medium=email&utm_term=0_940930e328-5247da06c4-389116456)
202 [Response_Recovery_2020_10_09&utm_medium=email&utm_term=0_940930e328-](https://coronavirus.berkeley.edu/dashboard/?utm_source=Response+and+Recovery&utm_campaign=5247da06c4-Response_Recovery_2020_10_09&utm_medium=email&utm_term=0_940930e328-5247da06c4-389116456)
203 [5247da06c4-389116456](https://coronavirus.berkeley.edu/dashboard/?utm_source=Response+and+Recovery&utm_campaign=5247da06c4-Response_Recovery_2020_10_09&utm_medium=email&utm_term=0_940930e328-5247da06c4-389116456) [Accessed October 1, 2020].
- 204 3. Perelson AS (2002) Modelling viral and immune system dynamics. *Nat Rev Immunol*
205 2(1):28–36.
- 206 4. Ho DD, et al. (1995) Rapid turnover of plasma virions and CD4 lymphocytes in HIV-1
207 infection. *Nature* 373:123–126.
- 208 5. Nowak MA, May RM (2000) *Virus Dynamics: Mathematical Principles of Immunology*
209 *and Virology* (Oxford University Press, Oxford, UK).
- 210 6. Ke R, Zitzmann C, Ribeiro RM, Perelson AS (2020) Kinetics of SARS-CoV-2 infection in
211 the human upper and lower respiratory tracts and their relationship with infectiousness.
212 *medRxiv*:2020.09.25.20201772.
- 213 7. Endo A, Abbott S, Kucharski AJ, Funk S (2020) Estimating the overdispersion in
214 COVID-19 transmission using outbreak sizes outside China. *Wellcome Open Res* 5:67.
- 215 8. Schwab J, Balzer LB, Geng E, Peng J, Petersen ML Local Epidemic Modeling for
216 Management and Action. Available at: <https://localepi.github.io/LEMMA/>.
- 217 9. Ferretti L, et al. (2020) Quantifying SARS-CoV-2 transmission suggests epidemic control
218 with digital contact tracing. *Science* 368(6491):eabb6936.
- 219 10. Wölfel R, et al. (2020) Virological assessment of hospitalized patients with COVID-2019.
220 *Nature* 581(7809):465–469.
- 221 11. Quicke K, et al. (2020) Longitudinal surveillance for SARS-CoV-2 RNA among
222 asymptomatic staff in five Colorado skilled nursing facilities: Epidemiologic, virologic
223 and sequence analysis. *medRxiv*. doi:10.1101/2020.06.08.20125989v1.
- 224 12. La Scola B, et al. (2020) Viral RNA load as determined by cell culture as a management
225 tool for discharge of SARS-CoV-2 patients from infectious disease wards. *Eur J Clin*
226 *Microbiol Infect Dis* 39(6):1059–1061.

227

228

229

230

231

232 **Legends for Supplementary Files 2-4.**

233 **Supplementary File 2. Averaged total cases saved and mean R_E reduction across group size**
234 **limit, symptomatic isolation, and surveillance testing NPIs.** Summarized model output from
235 100x simulations across all NPIs presented in Fig. 2 and Fig. 3, main text. Confidence intervals
236 represent 1.96*standard deviation in case reduction or R_E reduction.

237

238 **Supplementary File 3. Averaged total cases saved and mean R_E reduction across**
239 **symptomatic isolation, and surveillance testing NPIs, under regimes with and without**
240 **contact tracing.** Summarized model output from 100x simulations across all NPIs presented in
241 SI-Appendix, Fig. S3.

242

243 **Supplementary File 4. Averaged total cases saved and mean R_E reduction across combined**
244 **intervention approaches.** Summarized model output from 100x simulations across all NPIs
245 presented in Fig. 4, main text.

246

247 All other model output available as saved .Rdata files in our publicly-available Github
248 repository:

249 Brook CE, Northrup GR, Boots M (2020) Code for “Optimizing COVID-19 control with
250 asymptomatic surveillance testing in a university environment.” doi:10.5281/zenodo.4131223

251

252

253

254

255

256

257

258

259

260

261

262

263

264

265

266

267

268